The Plant Cell, Vol. 18, 3332–3345, November 2006, www.plantcell.org

A Ferroxidation/Permeation Iron Uptake System Is Required for Virulence in *Ustilago maydis* [W]

Heiko Eichhorn,[1,2] Franziska Lessing,[1,3] Britta Winterberg, Jan Schirawski, Jörg Kämper, Philip Müller,[4] and Regine Kahmann[5]

Max Planck Institute for Terrestrial Microbiology, D-35043 Marburg, Germany

In the smut fungus *Ustilago maydis*, a tightly regulated cAMP signaling cascade is necessary for pathogenic development. Transcriptome analysis using whole genome microarrays set up to identify putative target genes of the protein kinase A catalytic subunit Adr1 revealed nine genes with putative functions in two high-affinity iron uptake systems. These genes locate to three gene clusters on different chromosomes and include the previously identified complementing siderophore auxotroph genes *sid1* and *sid2* involved in siderophore biosynthesis. Transcription of all nine genes plus three additional genes associated with the gene clusters was also coregulated by iron through the Urbs1 transcription factor. Two components of a high-affinity iron uptake system were characterized in more detail: *fer2*, encoding a high-affinity iron permease; and *fer1*, encoding an iron multicopper oxidase. Fer2 localized to the plasma membrane and complemented an *ftr1* mutant of *Saccharomyces cerevisiae* lacking a high-affinity iron permease. During pathogenic development, *fer2* expression was confined to the phase of hyphal proliferation inside the plant. *fer2* as well as *fer1* deletion mutants were strongly affected in virulence. These data highlight the importance of the high-affinity iron uptake system via an iron permease and a multicopper oxidase for biotrophic development in the *U. maydis*/maize (*Zea mays*) pathosystem.

INTRODUCTION

The fungal pathogen *Ustilago maydis* causes smut disease of maize (*Zea mays*). The most prominent symptoms are plant tumors, and it is within these tumors that fungal hyphae proliferate and differentiate to diploid spores. *U. maydis* alternates between a unicellular yeast form and a dikaryotic filamentous form, which is infectious (Kahmann et al., 2000). The morphological transition is regulated by the *a* and *b* mating-type loci. The *a* locus codes for pheromones (Mfa1 and Mfa2) and the respective pheromone receptors (Pra1 and Pra2), whereas the *b* locus encodes a pair of transcription factors, *bE* and *bW*. These two proteins dimerize when derived from different alleles and then constitute the central regulator for sexual and pathogenic development (reviewed in Kahmann et al., 2000). Therefore, only cells that differ in *a* and *b* can form an infectious dikaryon.

Transcription of the *a* and *b* genes is controlled by a conserved mitogen-activated protein kinase cascade and through the cAMP pathway (Krüger et al., 1998; Kaffarnik et al., 2003; Müller et al., 2003). Both signaling pathways are required for discrete steps during pathogenic development (Gold et al., 1997; Müller et al., 1999, 2003; Krüger et al., 2000; Mayorga and Gold, 2001). cAMP signaling involves activation of the *Ustilago* adenylyl cyclase Uac1 via the G protein α subunit Gpa3 (Krüger et al., 1998). Subsequently, cAMP activates the cAMP-dependent protein kinase A (PKA) Adr1 by releasing the regulatory subunit *Ustilago* bypass of cyclase 1 (Ubc1) from the complex (Dürrenberger et al., 1998). Strains carrying deletions in either *uac1* or *gpa3* grow filamentously, indicating that cAMP represses filamentous growth (Barrett et al., 1993; Regenfelder et al., 1997). On the other hand, *ubc1* mutants that mimic a situation of high internal cAMP level have a multiple budding phenotype resulting from a cytokinesis defect (Gold et al., 1994). Mutants in which cAMP signaling is abolished are apathogenic, and the same holds for *ubc1* mutants. This demonstrates that regulated levels of PKA activity are essential for disease progression (Barrett et al., 1993; Gold et al., 1997; Dürrenberger et al., 1998).

cAMP signaling plays a key role during pathogenic development and cell morphogenesis in a variety of fungi, including human and plant pathogens (Alspaugh et al., 1997; Borges-Walmsley and Walmsley, 2000; D'Souza et al., 2001; Lee et al., 2003). *U. maydis* is one of the few fungal pathogens in which several downstream target genes of the cAMP pathway have been identified. These include the high mobility group domain transcription factor pheromone response factor 1 (Prf1), which binds to pheromone response elements. Prf1 is phosphorylated by Adr1 and is then able to activate transcription of the pheromone and receptor genes (Kaffarnik et al., 2003). Moreover, *Ustilago* kinase B–related 1 (Ukb1), a putative Ser/Thr protein kinase containing 30 putative PKA phosphorylation sites, is proposed to be a PKA target. Ukb1 has a role in lateral budding

[1] These two authors contributed equally to this work.
[2] Current address: Sandoz, Biochemiestrasse 10, 6250 Kundl, Austria.
[3] Current address: Leibniz Institute for Natural Product Research and Infection Biology, Beutenbergstrasse 11a, 07745 Jena, Germany.
[4] Current address: Eppendorf AG, Barkhausenweg 1, 22339 Hamburg, Germany.
[5] To whom correspondence should be addressed. E-mail kahmann@mpi-marburg.mpg.de; fax 49-6421178509.
The author responsible for distribution of materials integral to the findings presented in this article in accordance with the policy described in the Instructions for Authors (www.plantcell.org) is: Regine Kahmann (kahmann@staff.uni-marburg.de).
[W] Online version contains Web-only data.
www.plantcell.org/cgi/doi/10.1105/tpc.106.043588

and filamentous growth (Abramovitch et al., 2002). Similar to *ubc1* mutants, *ukb1* mutant strains infect their host but fail to induce tumors and are unable to complete sexual development (Abramovitch et al., 2002). Another direct target of PKA is the hyphal growth locus protein 1, which acts as a regulator for the switch between budding and filamentous growth (Dürrenberger et al., 2001). The identification of these genes is beginning to shed light on the processes that are regulated by cAMP in *U. maydis*.

Because of the general importance of cAMP signaling in pathogenesis, genome-wide expression profiling, serial analysis of gene expression, and PCR-select methods are currently applied to detect genes whose transcriptional profiles are affected by cAMP signaling (Labudova and Lubec, 1998; Irie et al., 2003, Lian et al., 2005). In *U. maydis*, serial analysis of gene expression recently was used to compare expression profiles of *ubc1* and *adr1* mutants, revealing a novel connection between cAMP and phosphate metabolism (Larraya et al., 2005). Here, we describe the use of genome-wide arrays for the detection of genes that are regulated via the cAMP pathway in *U. maydis*. We show that a large number of genes change expression upon induction of *adr1*. In this article, we concentrate on a set of coregulated genes that comprise three gene clusters involved in iron acquisition. One of these clusters is the previously identified ferrichrome biosynthesis gene cluster containing the complementing siderophore auxotroph genes *sid1* and *sid2* (Yuan et al., 2001). *U. maydis* is known to produce two siderophores, ferrichrome and ferrichrome A (Budde and Leong, 1989). Ferrichrome complexed iron is taken up and likely serves as an intracellular iron store, whereas ferrichrome A is thought to deliver iron to a membrane-bound iron reductase (Ecker and Emery, 1983; Ardon et al., 1997, 1998; Haas, 2003). In *U. maydis*, siderophore synthesis begins with the hydroxylation of Orn, and this step is catalyzed by an L-Orn N^5-monooxygenase encoded by *sid1* (Mei et al., 1993). *sid2* is a siderophore synthetase responsible for the synthesis of ferrichrome (Yuan et al., 2001). Both genes are under negative regulation by the iron-responsive GATA transcription factor Urbs1 (for *U. maydis* regulator of biosynthesis of siderophores) (An et al., 1997). Because *sid1* deletion mutants produce no siderophores and are not affected in virulence, iron acquisition during the biotrophic phase of *U. maydis* was postulated to use a different uptake system (Mei et al., 1993). Here, we show that the additional genes in the three identified gene clusters are also subject to regulation by iron through the Urbs1 transcription factor. Most importantly, we demonstrate that genes in one of the clusters code for a permease-based high-affinity iron uptake system that is required for virulence in *U. maydis*.

RESULTS

Identification of Coregulated Gene Clusters Involved in Iron Uptake

To identify genes whose expression depends on or is affected by the PKA Adr1, we performed a comparative genome-wide expression analysis. To this end, strain HE140 was generated, which expresses *adr1* encoding the catalytic subunit of the PKA under the control of the arabinose-inducible *crg1* promoter (Bottin et al., 1996). This experimental design was chosen because *Δadr1* strains have a severe morphological phenotype and are unstable (Dürrenberger et al., 1998, 2001). We chose to overexpress Adr1 rather than adding cAMP to avoid the additional induction of catalytic subunits of other PKAs present in *U. maydis* (Dürrenberger et al., 1998). The inducible *adr1* allele was integrated in a single copy into the *ip* locus of wild-type strain FB1 without affecting the native *adr1* allele. To assess the function of the introduced allele, the expression of *adr1* was compared with that of *pra1* by RNA gel blot analysis (Figure 1A). Expression of *pra1* is known to be activated by cAMP (Krüger et al., 1998; Kaffarnik et al., 2003) and served as a control. After induction of the *crg1* promoter, *adr1* expression increased significantly over time in strain HE140 but remained barely detectable in the FB1 control strain (Figure 1A). This finding illustrates that data were collected under conditions in which

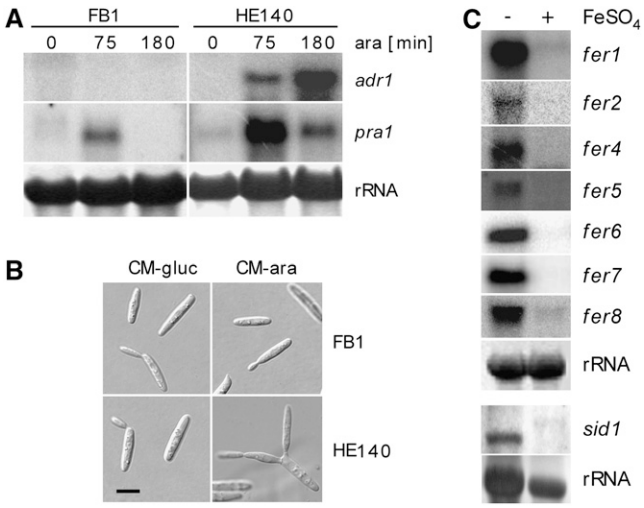

Figure 1. Characterization of Strain HE140 and Repression of Iron Uptake Cluster Genes by Iron.

(A) Induction of the *crg1* promoter in *U. maydis* strain HE140 (*a1b1*[P_{crg1}:*adr1*]*ip*^{s}) by arabinose (ara) induces *adr1* and *pra1* gene expression. Total RNA (10 μg) from the wild type (FB1) and strain HE140 isolated at 0, 75, and 180 min after the shift to arabinose-containing medium was loaded in each lane and probed successively with *pra1* and *adr1*. In the top panel, the same filter was probed successively with the genes indicated. In the middle panel, a separate filter was probed with *sid1*. Methylene blue staining of the rRNA is shown in the bottom panel as a loading control for the two separate filters used.

(B) Arabinose induction of *U. maydis* strain HE140 leads to unipolar budding. Light microscopy is shown for wild-type FB1 and HE140 strains grown in complete medium (CM) (Holliday, 1974) supplemented with 1% glucose (left) and shifted for 180 min to CM containing 1% arabinose (right). Bar = 5 μm.

(C) Iron represses the expression of genes localized in the high-affinity iron uptake clusters. Total RNA (10 μg) from wild-type strain FB1 grown in minimal medium (Sundström, 1964) without (−) and with (+) the addition of 10 μM $FeSO_4$ was used in each lane. Blots were successively probed with gene-specific probes as indicated at right. Methylene blue staining of the rRNA is shown as a loading control at bottom.

adr1 was overexpressed. *pra1* was strongly upregulated 75 min after induction of *adr1* (Figure 1A) and declined at 180 min after induction. In FB1 wild-type cells subjected to the same shift conditions, one could also observe an increase in *pra1* transcript levels after 75 min in arabinose (Figure 1A). This increase was transient, however, and disappeared after 180 min (Figure 1A). This suggests that the transient peak seen in HE140 and in FB1 is attributable to the medium shift. One possibility is that this reflects the release from catabolite repression. Because the pheromone response factor *prf1*, the main regulator of *pra* gene expression, is transcribed with the same efficiency in medium containing glucose or arabinose (Hartmann et al., 1999), one would have to assume additional regulatory circuits in such a scenario. Also, cells lacking the regulatory subunit *ubc1* show high levels of *a* gene expression in glucose-containing medium, which makes it unlikely that glucose is repressing those genes that are activated through the cAMP pathway. At 180 min after induction, 7% of all HE140 cells had started to form a second bud at the same pole or showed lateral buds (Figure 1B; data not shown), two phenotypic alterations induced by high cAMP levels (Gold et al., 1994). At later time points, nearly all cells displayed this phenotype (data not shown). In FB1, no changes in morphology were noted at any time point (Figure 1B). These results demonstrate that strain HE140 is suited to follow the events occurring after activation of the cAMP pathway.

For expression profiling, Affymetrix arrays representing 93% of all *U. maydis* genes were used (see Methods). Except for the zero time points, at which only two biological replicates were used, all subsequent time points were analyzed in biological triplicates to exclude variations in culture conditions and handling. HE140 and FB1 strains were grown to log phase ($OD_{600} = 0.5$) in CM containing glucose. Expression of *adr1* was activated by shifting the cells to CM containing arabinose. Before induction as well as 75 and 180 min after induction, cells were harvested and analyzed. Among a set of 847 genes that were differentially regulated in HE140 and FB1 (see Supplemental Figure 1 and Supplemental Table 1 online), we identified a subset of 407 coregulated genes (see Methods for details; see Supplemental Figure 1 and Supplemental Table 1 online). The coregulated genes had in common that their expression values in strain HE140 stayed at a high level 75 min after switching on *adr1* and declined at 180 min. In the wild-type strain FB1, expression levels of these genes declined significantly already after 75 min and increased again after 180 min (see Supplemental Figure 1 and Supplemental Table 1 online). In this group, we identified nine genes that not only exhibited coregulation but also were found to be located in three gene clusters on chromosomes 1, 2, and 4 of the *U. maydis* genome (Figure 2, dark gray arrows). Among the 10 genes were *sid1* and *sid2*, already known to be part of the ferrichrome biosynthesis gene cluster (Yuan et al., 2001). Surprisingly, most of the other eight genes in the clusters were also predicted to have a function in iron uptake. They were designated *fer* (Fe-regulated) genes. In the cluster on chromosome 2, another putative siderophore peptide synthetase gene, *fer3*, with 25.9% identity to *sid2*, is present (Figure 2). We presume *fer3* to encode the peptide synthetase catalyzing ferrichrome A biosynthesis. In the gene cluster on chromosome 2, we also found an acylase gene, *fer5*, that displays similarity to an acyltransferase found in the putative ferrichrome A biosynthetic

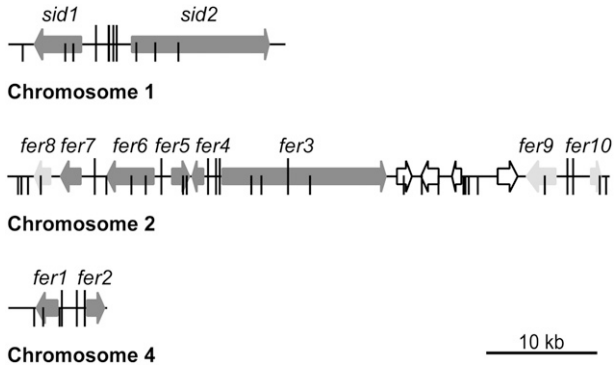

Figure 2. Physical Map of Three Coregulated Iron Uptake Clusters.

The coregulated genes localize to clusters on three chromosomes of *U. maydis*. Coding regions are represented by arrows indicating the direction of transcription. Dark gray arrows, coregulated genes involved in iron uptake identified by arabinose induction of HE140; light gray arrows, additional genes identified as being coregulated by iron and Urbs1; open arrows, genes not belonging to the coregulated iron uptake clusters (um01435, um01436, um01437, um01438, and um01442 on chromosome 2 and um00107 on chromosome 4). Urbs1 binding sites (G/TGATAA) as defined by An et al. (1997) are depicted as vertical bars. Sites carrying the extended consensus motif ATCG/TGATAAA/G identified in this study are marked with long vertical bars.

gene cluster of *Omphalotus olearius* (Welzel et al., 2005) (Table 1). Fer5 could potentially carry out acylation of N^5-hydroxy-L-Orn residues in ferrichrome A. Located between the *fer3* and *fer5* genes is *fer4*, encoding a putative enoyl-CoA isomerase (Figure 2, Table 1). This enzyme might be responsible for the *trans* configuration of the acyl chain attached to the hydroxy-Orn. In addition, two genes, *fer6* and *fer7*, encoding major facilitator proteins are part of this cluster (Figure 2, Table 1). Fer7 is related to a likely siderophore transporter, Str3, from *Schizosaccharomyces pombe* (39% identity) and to Sit1p, a siderophore transporter from *Saccharomyces cerevisiae* (25% identity), suggesting a function in siderophore uptake. Fer6 shows high similarity with multispecific ATP binding cassette transporters and could have a role in the uptake of alternative ferric iron complexes. The two coregulated genes found on chromosome 1, *fer1* and *fer2*, encode a putative ferroxidase and a high-affinity ferric permease, respectively (Figure 2, Table 1). Genes in all three clusters could conceivably encode components of two distinct high-affinity iron uptake systems (Kosman, 2003). We refer to these three gene clusters as iron uptake clusters.

Genes in the Iron Uptake Clusters Are Iron Regulated

The *sid1* and *sid2* genes are repressed under high-iron conditions by the GATA factor Urbs1 (Mei et al., 1993; An et al., 1997; Yuan et al., 2001). Therefore, we analyzed the intergenic regions of the *fer* genes for potential Urbs1 binding sites (G/TGATAA). Elements with a perfect match to this site could be identified in the intergenic regions of all iron cluster genes (Figure 2). On these grounds, it was likely that the *fer* genes are regulated by iron through Urbs1. To study possible iron effects on *fer* gene expression, RNA gel blot analysis was performed with wild-type cells (FB1) grown either in low-iron medium or in the same

Table 1. Annotation of Genes in the Iron Uptake Clusters

Gene	No.[a]	Protein Length (Amino Acids)[a]	Putative Function	Closest Known Homolog (Accession No.), Organism	Amino Acid Identity (%)[a]
fer1[b]	um00105	629	Iron multicopper oxidase	Lac1 (Q6E0Y2), *Auricularia polytricha*	51.7
fer2[b]	um10023	486	High-affinity iron permease	CaFtr1 (Q5KJQ5), *Cryptococcus neoformans*	35.7
fer3[c]	um01434	4830	Siderophore peptide synthetase	*SidC* (*Q7Z8P4*), *Aspergillus nidulans*	33.6
fer4[c]	um01433	274	Enoyl-CoA isomerase/hydratase	BH1135 (Q9KDS6), *Bacillus halodurans*	47.7
fer5[c]	um01432	427	Acyltransferase	Ato1 (AAX49354), *Omphalotus olearius*	48.9
fer6[c]	um01431	1397	Multidrug resistance protein	Yor1 (Q5KED3), *Cryptococcus neoformans*	39.7
fer7[c]	um11339[d]	659	Siderophore transporter	Str3 (Q92341), *Schizosaccharomyces pombe*	39.2
fer8[c]	um11338[d,e]	398	Unknown	CNI00360 (Q5KC39), *Cryptococcus neoformans*	35.0
fer9[f]	um01439	715	Ferric reductase	Fre3 (NP_015026), *Saccharomyces cerevisiae*	24.3
fer10[f]	um11873	117	Unknown	RpsL (Q9Z9L9), *Bacillus halodurans*	22.3
fer11[f]	um01441	304	Unknown	Psyr_1077 (Q4ZXI9), *Pseudomonas syringae*	44.3
sid1[g]	um10188[h]	649	L-Orn N^5-monooxygenase	SidA (Q5SE95), *Aspergillus fumigatus*	32.2
sid2[i]	um10189	4114	Ferrichrome siderophore peptide synthetase	*SidC* (*Q7Z8P4*), *Aspergillus nidulans*	26.6

[a] Data from the MIPS database (http://mips.gsf.de/genre/proj/ustilago/).
[b] Accession number BK004082.
[c] Accession number BK004083.
[d] *fer7* and *fer8* are two independent genes as verified by RT-PCR.
[e] Both annotated introns verified by RT-PCR and sequencing.
[f] Accession number BN000978.
[g] Accession number M98520.
[h] Both annotated introns verified by RT-PCR.
[i] Accession number U62738.

medium in the presence of 10 μM $FeSO_4$ (Sundström, 1964). *sid1* was included as a control to confirm the observation that a transcript of 2.3 kb dominates under low-iron conditions, whereas a larger transcript of lower abundance is found in medium containing 10 μM iron (Mei et al., 1993) (Figure 1C). When cells were grown in low-iron medium, a high expression level was observed for all *fer* genes tested. By contrast, *fer* gene transcripts in RNA prepared from cells grown in the same medium containing iron could barely be detected (Figure 1C). This finding illustrates that the *fer* genes are repressed by iron, as was shown previously for *sid1* and *sid2* (Mei et al., 1993; Yuan et al., 2001). We can also infer from these results that the CM used to grow cells for the array experiments (see Supplemental Figure 1 and Supplemental Table 1 online) represents a medium limited in iron, which was experimentally verified.

To analyze a potential role of Urbs1 in regulating the identified *fer* genes, we isolated an *urbs1* deletion mutant (BW12) and performed comparative array analysis. Transcript profiles of wild-type strain FB1 were generated from cells grown in CM in the presence and absence of iron, whereas transcript patterns of BW12 were determined from cells grown in CM in the presence of iron. Genes repressed by iron and Urbs1 were identified as being coregulated. A set of 67 genes showed a fold change > 1.5 in the comparison of FB1 and BW12 grown in the presence of 10 μM $FeSO_4$ as well as in the comparison of FB1 grown with and without iron supplement (see Supplemental Table 2 online). For all *fer* genes and *sid1* and *sid2*, regulation by Urbs1 could be shown (see Supplemental Table 2 online). This analysis also revealed the existence of three additional *urbs1* and iron-repressed genes, of which one is located downstream of *fer7* (termed *fer8*) and two are located downstream of *fer3* (termed *fer9* and *fer10*) (Figure 2, light gray arrows on chromosome 2). These genes are separated from *fer3* by a group of four genes of unknown function, which are not regulated by iron (Figure 2). *fer9* is related to the iron reductase *frp1* from *S. pombe*, whereas *fer10* is related to genes of unknown function in other organisms (Table 1). Except for *fer8*, which codes for a hypothetical protein (Table 1) whose relation to iron acquisition is unclear, the additional *fer* genes show perfect matches to the Urbs1 binding site in their respective promoter regions (G/TGATAA; Mei et al., 1993). However, the four genes in the clusters that are not regulated by Urbs1 also show this sequence motif either in their promoters or in their coding regions (Figure 2; see Discussion). In addition to the 12 *urbs1* and iron-regulated genes in the three iron gene clusters, we identified 55 nonclustered genes as being *urbs1* and iron regulated (see Supplemental Table 2 online).

cAMP and Iron Regulate the Expression of the Iron Gene Clusters

To learn more about the connection between repression by iron and activation by cAMP, we analyzed the expression of several *fer* genes and of *sid1* in a *Δuac1* mutant lacking adenylyl cyclase (Figure 3A). *fer2* transcripts could not be detected in FB1*Δuac1*

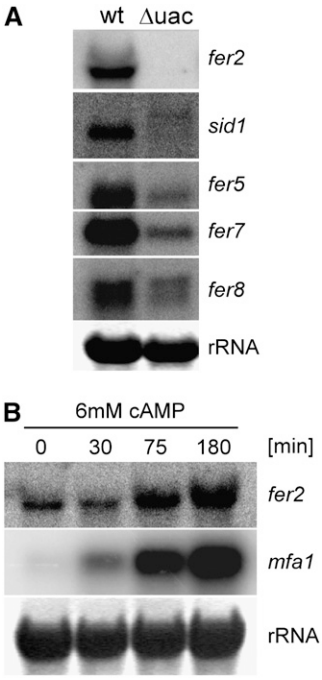

Figure 3. Expression of Genes in the Iron Uptake Clusters Responds to cAMP Signaling.

(A) The expression of genes in the iron uptake clusters is reduced in a *U. maydis* strain lacking the regulatory subunit (Uac1) of the cAMP-activatable protein kinase C (Adr1). Total RNA (10 μg) isolated from wild-type strain FB1 (wt) and strain FB1Δuac1 (Δuac) grown in CM (Holliday, 1974) containing glucose was applied to each lane. The blot was probed sequentially with the probes indicated at right. Methylene blue staining of the rRNA is shown as a loading control at bottom.

(B) Expression of *fer2* can be induced by cAMP feeding. RNA from wild-type strain FB1 grown in CM (Holliday, 1974) containing glucose was isolated at 0, 30, 75, and 180 min after stimulation with 6 mM cAMP. Total RNA (10 μg) was loaded in each lane. The blot was probed successively with probes against *fer2* and *mfa1*. Methylene blue staining of the rRNA is shown as a loading control at bottom.

strains, whereas expression of *fer2* was seen in FB1 wild-type cells that were grown in the same medium (Figure 3A). These results show that *fer2* expression completely depends on an intact cAMP pathway. For all other *fer* genes tested, as well as for *sid1*, lower transcript levels were seen in the Δ*uac1* strain compared with the wild type (Figure 3A), which illustrates that the full expression of these genes also requires an intact cAMP pathway. For *sid1*, low amounts of a 2.7-kb transcript were detected in FB1Δ*uac1*, whereas a more abundant 2.3-kb transcript was visible in corresponding wild-type cells (Figure 3A). This finding reinforces the notion that CM is iron-limited and demonstrates that the smaller transcript seen under these iron-limiting conditions (Mei et al., 1993) requires the presence of an intact cAMP pathway. We also investigated the expression of the *fer* genes after cAMP feeding (Figure 3B; data not shown). In this experiment, the expression level of the pheromone gene *mfa1*, which is known to increase upon cAMP addition (Figure 3B), served as a control (Krüger et al., 1998). Upon addition of 6 mM cAMP, expression of *fer2* was stimulated (Figure 3B). However, none of the other *fer* genes tested (*fer1*, *-4*, *-5*, *-6*, *-7*,and *-8*) responded with a significant induction (data not shown).

Characterization of the High-Affinity Iron Permease *fer2*

Because the high-affinity iron uptake system involving siderophores was shown to be dispensable for the pathogenicity of *U. maydis* (Mei et al., 1993), we considered the possibility that high-affinity uptake via an iron permease might be required for virulence. *fer2* codes for a putative protein of 486 amino acids and shows significant homology with other fungal high-affinity iron permeases, such as Ftr2p from *Candida albicans* (44% identity) and Ftr1p from *S. cerevisiae* (35% identity). Inspection of the amino acid sequence identified a highly conserved REGLE motif in Fer2, which is located between amino acids 262 and 268 and is essential for iron uptake by iron permeases (Fang and Wang, 2002). To investigate whether Fer2 is functional, we tested the ability of *U. maydis fer2* to complement an *FTR1* mutant of *S. cerevisiae. FTR1* mutant strains have an iron(III)-dependent growth defect that can be rescued by expressing *FTR1* from a centromeric plasmid under the control of a galactose-inducible promoter (Ramanan and Wang, 2000). Transformants of strain BY4741Δ*FTR1* carrying the empty vector YCplac111-G/T were unable to grow on low-iron plates even in the presence of galactose but grew well when iron was provided at higher concentrations (Figure 4A). The same strain transformed with either pfer2 or pFtr1 was unable to grow on low-iron plates containing glucose but showed growth on low-iron plates containing galactose (Figure 4A). This finding illustrates that *U. maydis fer2* is able to complement the growth defect of an *FTR1* strain of *S. cerevisiae* efficiently and thus encodes a functional iron permease.

Pathogenic Development Is Attenuated in *fer2* Deletion Mutants

To analyze the function of *fer2*, we constructed strains in which the entire open reading frame was replaced by a hygromycin resistance cassette by homologous recombination (FB1Δfer2#1 and FB2Δfer2#4). When compatible mixtures of Δ*fer2* strains were spotted on CM plates containing charcoal, dikaryotic filaments developed as efficiently as in compatible mixtures of wild-type strains (data not shown). However, when grown on low-iron plates, Δ*fer2* mutants were reduced in growth compared with the wild type (Figure 4B). This illustrates that the high-affinity iron uptake system based on the iron permease confers a selective growth advantage under iron(III)-limiting conditions.

To investigate the consequences of the deletion of *fer2* on pathogenic development, 5-d-old maize seedlings were inoculated with compatible mixtures of *fer2* deletion strains. With respect to tumor formation, compatible mixtures of Δ*fer2* strains showed a significant reduction of disease symptoms compared with infections with compatible wild-type strains (Figure 5). After 12 d, on average 31.5 ± 1.8% of plants infected with a mixture of Δ*fer2* mutants showed tumor development, and only a single plant was killed. In comparison, 91.6 ± 5.1% of all plants infected with corresponding wild-type strains produced tumors, and in these infections plant death was observed in 59% of all cases.

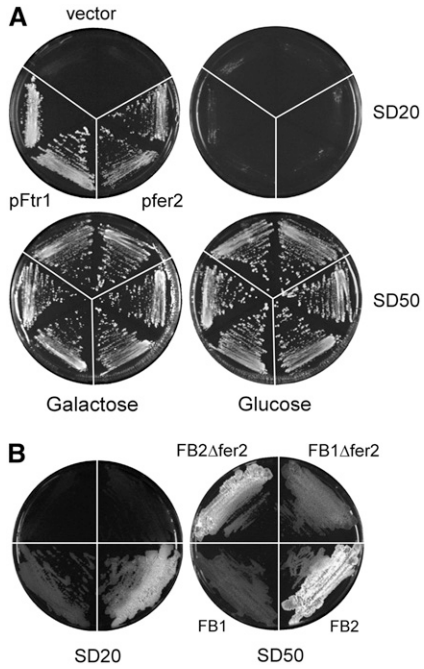

Figure 4. Complementation of the Iron-Dependent Growth Defect of the *S. cerevisiae* Δ*FTR1* Mutant and the Iron-Dependent Growth Defect of *U. maydis* Δ*fer2* Strains.

(A) The iron-dependent growth defect of the *S. cerevisiae* Δ*FTR1* mutant can be complemented by expression of *fer2*. The *S. cerevisiae FTR1* mutant was transformed with empty vector YCplac111-G/T (vector), a plasmid expressing *fer2* of *U. maydis* (pfer2), or a plasmid expressing *FTR1* (pFtr1) under the control of the galactose-inducible *GAL1* promoter. Two independent transformants were streaked on SD plates (Ramanan and Wang, 2000) containing $FeCl_3$ (20 μM [SD20], top; or 50 μM [SD50], bottom) and galactose (2%; left) or glucose (2%; right). The plates were incubated for 3 d at 28°C.

(B) *U. maydis* Δ*fer2* strains are attenuated in growth on iron-limiting plates. Wild-type strains FB1 and FB2 and isogenic *fer2* deletion strains were streaked on SD plates (Ramanan and Wang, 2000) containing glucose (2%) and $FeCl_3$ to either 20 μM (SD20) or 50 μM (SD50). The plates were incubated for 3 d at 28°C. Differences in colony morphology between FB1 and FB2 strains and their derivatives are attributable to stronger filamentation of strains with the FB2 genetic background.

When a Δ*fer2* strain was crossed with a compatible wild-type strain, symptom development was restored almost to wild-type levels, illustrating complementation of the defect (Figure 5).

Fungal development after infection was also investigated microscopically. Although formation of appressoria-like structures was indistinguishable in infections with Δ*fer2* and wild-type strains (Figure 6A), 6 d after infection a reduction in fungal proliferation was observed in infections with the Δ*fer2* mutant compared with wild-type strains, and this difference in proliferation was maintained also at later stages (Figure 6A; data not shown). At day 12, wild-type strains had produced large amounts of mature spores, whereas in infections with *fer2* mutant strains, spores were only rarely detected (Figure 6A) but were viable (data not shown). These results indicate that the Δ*fer2* mutants are attenuated during growth in planta. Δ*fer2* mutants were even more attenuated in virulence when maize yellow stripe mutants (*ys1*) lacking an iron siderophore transporter (Curie et al., 2001) were infected. Although wild-type strains could cause normal disease symptoms on these host plants (of 20 infected plants, all produced tumors at day 12 after infection), Δ*fer2* mutants were able to elicit anthocyanin production but completely failed with respect to tumor induction (of 21 infected plants, 17 showed anthocyanin induction but none developed tumors 12 or more days after infection).

To reinforce the crucial role of the permease-based high-affinity iron uptake system for virulence in *U. maydis*. We also generated a deletion of the *fer1* gene encoding a putative iron multicopper oxidase. Homologs of this gene product have been shown to reoxidize Fe^{2+} to Fe^{3+} in other systems and thereby provide the substrate for the permease (Kosman, 2003). When maize seedlings were coinoculated with a compatible mixture of *fer1* deletion strains, virulence was reduced significantly (43.2 ± 2.3% compared with 91.6 ± 5.1% for the wild type; Figure 5). Virulence could be largely restored by coinoculation of a *fer1* deletion strain with a compatible wild-type strain (Figure 5). *fer1*

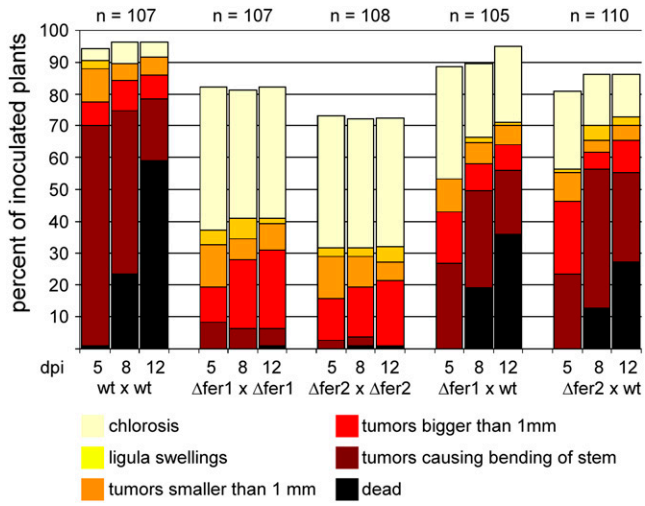

Figure 5. *U. maydis* Strains Carrying Deletions in the *fer2* and *fer1* Genes Are Affected in Virulence.

Time course of disease progression in infections with wild-type and Δ*fer1* and Δ*fer2* deletion strains. Five-day-old maize seedlings were inoculated with a mixture of wild type (wt) strains FB1 and FB2, a mixture of compatible *fer2* deletion mutants (Δfer2), a mixture of compatible *fer1* deletion mutants (Δfer1), or mixtures of *fer1* or *fer2* deletion strains with the compatible wild-type strain. Disease progression was monitored at 5, 8, and 12 d after infection (dpi). Each plant was grouped into one of six categories according to the most severe symptom displayed. The categories were, in order of severity: chlorosis (yellow), ligula swellings (light orange), tumors smaller than 1 mm (dark orange), tumors larger than 1 mm (red), tumors causing bending of the stem (brown), and dead plants (black). The values shown are the sum of three independent experiments expressed as percentage of the total number of inoculated plants (n). In each experiment, 30 to 38 plants were inoculated for each strain combination.

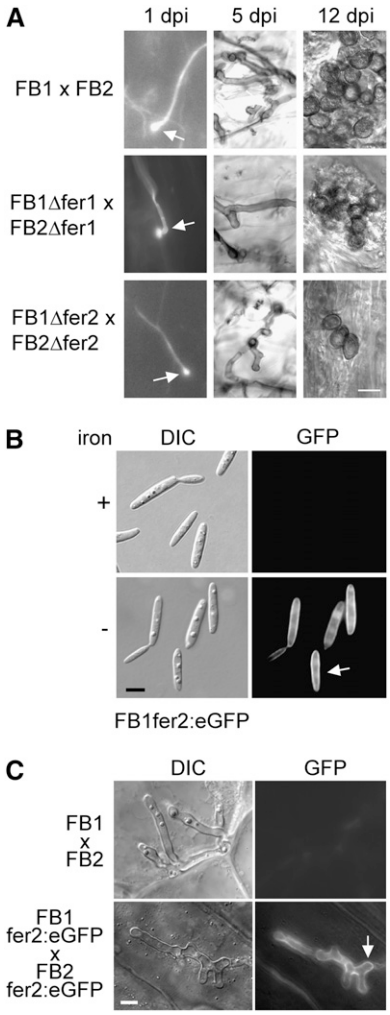

Figure 6. Biotrophic Development of Δ*fer2* Strains and Localization of the Fer2:eGFP Fusion Protein.

(A) Δ*fer1* and Δ*fer2* strains penetrate but show limited growth and rare spore formation. Plants were infected with a mixture of wild-type strains (FB1 × FB2), a mixture of *fer1* deletion strains (FB1Δfer1 × FB2Δfer1), or a mixture of *fer2* deletion strains (FB1Δfer2 × FB2Δfer2). Fungal structures were observed at 1, 5, and 12 d after infection (dpi) after staining with calcofluor and visualization with fluorescence microscopy (left panels), after staining with Chlorazole black E (middle panels), or without staining (right panels) and visualization by light microscopy (middle and right panels). At 1 d after infection, appressoria (arrows) were observed for all strain combinations (left panels). The sample showing an appressorium of the Δ*fer1* deletion strains was treated with chloroform before calcofluor staining. At 5 d after infection, fewer mycelial structures were observed in infections with *fer1* and *fer2* deletion strains than in infections using wild-type strains (middle panels). At 12 d after infection, fully melanized spores were readily observed in infections using wild-type strains but were rarely found in infections using *fer1* or *fer2* deletion strains (right panels). Bar = 10 μm for all panels.

(B) The Fer2:eGFP fusion protein is expressed under low-iron conditions and localizes to the plasma membrane. The *U. maydis* strain FB1fer2:eGFP was grown in minimal medium (Sundström, 1964) in the absence or presence of 10 μM $FeSO_4$ (iron). Light microscopy images are shown in the left panel (differential interference contrast [DIC]), and fluorescence images are depicted at right (GFP). Bar = 5 μm.

(C) The Fer2:eGFP fusion protein is expressed at a specific stage during biotrophic growth. Plants were infected with a combination of wild-type strains (FB1 × FB2) or strains carrying the *fer2:egfp* fusion (FB1fer2:eGFP × FB2fer2:eGFP). Fungal hyphae within the plant tissue were visualized at 6 d after infection by light microscopy (differential interference contrast [DIC]; left panels) or by epifluorescence (GFP; right panels). Bar = 5 μm.

mutants were attenuated in growth and spore formation (Figure 6A) and thus behave similar to Δ*fer2* mutant strains.

A Functional Fer2:GFP Fusion Protein Localizes to the Plasma Membrane and Is Expressed at a Specific Stage during Plant Colonization

To analyze the expression of *fer2* during biotrophic growth and to study the localization of the *fer2* gene product, we fused enhanced green fluorescent protein (eGFP) to the C terminus of Fer2. The respective strains FB1fer2:eGFP and FB2fer2:eGFP were as proficient in tumor induction as their progenitor strains, which illustrates that the fusion protein is functional (data not shown). In low-iron medium, the fusion protein localized mainly to the plasma membrane (Figure 6B). When cells were grown in medium supplemented with iron, no GFP fluorescence was detectable (Figure 6B). To study the expression pattern during infection, plants were inoculated with a mixture of FB1fer2:eGFP and FB2fer2:eGFP grown in YEPSL medium (see Methods), which provides iron in sufficient concentration to repress *fer2* gene expression (data not shown). *fer2* expression could not be detected in infection structures on the leaf surface and during biotrophic growth until day 5 after infection (data not shown). On day 6, characteristic staining of the plasma membrane was observed in lobed, branched hyphae (Figure 6C). This stage has been described to precede sporulation (Snetselaar and Mims, 1994; Banuett and Herskowitz, 1996). At later stages, expression of *fer2* could no longer be detected (data not shown). These data indicate that starting with cells that are pregrown in iron-containing medium, *fer2* gene expression is restricted to a narrow phase of fungal development within the plant tissue.

DISCUSSION

The use of genome-wide arrays coupled with the analysis of mutants has enabled us to identify a cluster of coregulated genes for two high-affinity iron uptake systems in *U. maydis*. Although the siderophore system is dispensable for pathogenesis (Mei et al., 1993), a ferroxidase/permease system was shown to be required for full virulence.

Iron Uptake Gene Clusters

The gene clusters identified in this study reside on three chromosomes and contain mostly genes with predicted functions in

two high-affinity iron uptake systems. *U. maydis* is known to produce two siderophores, ferrichrome and ferrichrome A (Wang et al., 1989). Both are cyclic peptides that are nonribosomally produced and likely require specific transporters for excretion as well as plasma membrane permeases for uptake (Kosman, 2003). The genes in clusters on chromosomes 2 and 4 could potentially be involved in the biosynthesis and transport of siderophores. Of particular interest is *fer3*, encoding the putative peptide synthetase for the biosynthesis of ferrichrome A. To date, only three fungal peptide synthetase genes involved in siderophore biosynthesis have been functionally characterized (*sid2* from *U. maydis* [Yuan et al., 2001], *sidC* from *Aspergillus nidulans* [Eisendle et al., 2003; Haas, 2003], and *sib1* from *S. pombe* [Schwecke et al., 2006]). Based on the domain architecture of Fer3 (Schwecke et al., 2006), we anticipate that this enzyme is responsible for the synthesis of ferrichrome A. This is also supported by the finding of an iron-regulated putative ferrichrome A biosynthetic gene cluster in *O. olearius* (Welzel et al., 2005), which contains a peptide synthetase with higher identity to *fer3* (29.8%) than to the ferrichrome synthetase *sid2* (24.7%). Clustering of a siderophore peptide synthetase with an L-Orn N^5-monooxygenase is a principle realized not only in *U. maydis* (Yuan et al., 2001) but also in *S. pombe*, *Aureobasidium pullulan*s, and *O. olearius* (Haas, 2003; Welzel et al., 2005). In *O. olearius*, the cluster is extended by an acyltransferase gene predicted to be involved in the modification of N^5-hydroxy-Orn, similar to the arrangement found in the cluster on chromosome 2 of *U. maydis*. Novel is the large gene cluster on chromosome 2 of *U. maydis*, which combines many genes for biosynthesis as well as for the transport of siderophores. Clustering of such activities has been observed only in *A. pullulans*, in which a single putative ATP binding cassette transporter gene maps between the siderophore synthetase and the L-Orn N^5-monooxygenase genes (accession number U85909). Extensive clustering of siderophore biosynthesis and transport genes is a hallmark of pathogenic bacteria, in which the respective genes are found in pathogenicity islands (Schryvers and Stojiljkovic, 1999; Carniel, 2001; Rodriguez and Smith, 2003).

The third group of genes identified in this study is clustered on chromosome 1 and includes the genes for a high-affinity ferric permease as well as a putative iron multicopper oxidase. *fer2* permease of *U. maydis* has no paralogs elsewhere in the genome and can complement the defects of a Δ*FTR1* mutant of *S. cerevisiae* as efficiently as the yeast *FTR1* gene, demonstrating that *fer2* functions as a genuine ferric permease. Further experiments will be necessary to show whether Fe^{2+} or Fe^{3+} is the preferred substrate of *fer2*. The situation in which genes encoding an iron multicopper oxidase and a ferric permease are clustered is not unique to *U. maydis*; it is also found in *Neurospora crassa*, *S. pombe*, and *Cryptococcus neoformans* (Askwith and Kaplan, 1997; Lian et al., 2005). The iron permease and oxidase form a complex and are part of an indirect ferrous uptake system in which a relatively unspecific plasma membrane reductase accumulates and reduces Fe^{3+} present in the growth medium. The resulting Fe^{2+} is then reoxidized by the multicopper oxidase before transport by the permease (Kosman, 2003). Interestingly, in *U. maydis*, an iron-regulated putative reductase gene (*fer9*) is also contained in the cluster on chromosome 2.

Regulation of the Iron Cluster Genes

The iron cluster genes were identified because they appear to be coregulated when the PKA Adr1 is induced. The link to cAMP signaling could be substantiated for several *fer* genes tested as well as for *sid1* (i.e., these genes displayed reduced transcript levels in a strain lacking adenylyl cyclase). However, *fer2* was the only gene in which an increase in transcript levels was seen after cAMP feeding. In yeast, one of the three PKA catalytic subunits, Tpk2p, represses the transcription of genes involved in high-affinity iron uptake, which includes the genes encoding ferric reductases, an iron permease, as well as the putative siderophore iron transporter Sit1p (Robertson et al., 2000). For some of these genes, it has been shown that they are transcriptionally activated by *AFT1* (for activator of ferrous transport) under conditions of iron deprivation (Yamaguchi-Iwai et al., 1996). In contrast with this positive regulation, *sid1* and *sid2* genes in *U. maydis* are negatively controlled by the GATA transcription factor Urbs1 in the presence of iron (Voisard et al., 1993; An et al., 1997). Urbs1-mediated repression is alleviated under low-iron conditions (Voisard et al., 1993). We show here that all genes in the iron gene clusters are also upregulated when iron is limiting and that this regulation occurs through Urbs1. Within the three iron clusters, 44 putative Urbs1 binding sites were identified, and a closer inspection revealed an extended conserved binding motif (ATCG/TGATAAA/G) for sites that are overrepresented in intergenic regions (Figure 2, long vertical bars). Therefore, we speculate that Urbs1 recognizes this more extended binding site. Most of the iron cluster genes contain this extended motif in their promoters (Figure 2). Only *fer8* lacks this site, which may indicate that Urbs1 regulation can occur at a distance or may be indirect. Of the additional 55 Urbs1 and iron-regulated genes identified by array analysis, only four have the extended binding motif (see Supplemental Table 2 online). This finding could indicate that many of the genes, which are upregulated in *urbs1* deletion strains under high-iron conditions, are not direct Urbs1 targets. It is conceivable that their expression in *urbs1* mutants responds to uncontrolled iron uptake, which could induce a stress response. Such an observation has been made in *SFU1* (for suppressor of ferric uptake) mutants of *C. albicans*, which lack the Urbs1 ortholog (Lan et al., 2004).

How could cAMP signaling and iron regulation be connected? Urbs1 transcription is not affected by iron (Voisard et al., 1993), which makes it likely that primary levels of control occur post-transcriptionally. Current models assume a direct role of iron in determining the activity of Urbs1 and related factors (Rutherford and Bird, 2004). In this respect, it may not be a coincidence that Urbs1 has eight putative PKA phosphorylation sites (PROSITE prediction; http://www.expasy.org). It is thus conceivable that the phosphorylation of Urbs1 could affect its DNA binding affinity or interaction with other regulatory proteins. In *S. pombe*, the Urbs1 ortholog Fe protein1 was shown to interact with Tup11 and Tup12 proteins, which are proposed to act as corepressors (Znaidi et al., 2004). The observed induction of *fer2* after cAMP addition and the absence of *fer2* transcripts in a *Δuac1* strain would fit such a model. However, it is also clear that the other *fer* genes are subject to a more complex pattern of control, as they showed only reduced expression in the *Δuac1* strain and none of them could be induced by cAMP feeding alone. During growth

within the plant, *fer2* expression could be detected only in a defined time window at ~6 d after infection. Because the inoculum for this experiment was grown under iron-repressing conditions, we cannot exclude the possibility that cells may have used up their internal iron supplies before switching on the permease uptake system. In *S. cerevisiae*, this has been shown to require four cell doublings (Georgatsou and Alexandraki, 1994). We do not currently know whether the observed expression of *fer2* at this stage is attributable to iron deprivation or reflects high internal cAMP levels.

Fer2 and Fer1 Are Virulence Factors

When maize plants are infected with a compatible combination of wild-type strains, tumor development is seen in >90% of infected plants and a high percentage of these plants die after a period of 12 d. In infections with Δ*fer2* as well as with Δ*fer1* mutants, fewer plants develop tumors, and these remain relatively small. As a consequence, plant death is rarely observed. On these grounds, both genes are virulence factors. *fer2* and *fer1* mutants are not affected in early development on the leaf surface; they form appressoria and penetrate. However, after 5 d, when wild-type dikaryons have heavily ramified the plant tissue, accumulations of fungal cells are rarely seen in the *fer1* and *fer2* mutants. As a likely result of this, both mutants produce significantly fewer spores than wild-type plants. Interestingly, Δ*fer2* strains are more virulent on a wild-type host than on the maize *ys1* mutant, which has a defect in Fe(III) phytosiderophore uptake (Curie et al., 2001). This finding indicates that permease-based high-affinity iron uptake is sufficient for iron acquisition in wild-type strains even under conditions of low iron availability. Neither the high-affinity siderophore system nor low-affinity uptake involving a ferrous permease (for which um05420 is a possible candidate) can substitute for ferroxidation/permeation-mediated uptake in the *fer2* mutant. Thus, the ferroxidation/permeation system is decisive for iron acquisition during plant colonization by *U. maydis*. This is demonstrated by the unaffected virulence of two different mutants unable to produce siderophores: the Δ*sid1* mutant, which lacks the first committed enzyme for siderophore biosynthesis and hence lacks both siderophores (Mei et al., 1993), and a mutant in which both siderophore synthetase genes are deleted (B. Winterberg, unpublished data). This finding could indicate that components of the system for iron uptake via siderophores (Winkelmann, 2002) are not expressed during biotrophic growth. In this scenario, the siderophore biosynthesis and transport genes would have to be under separate control from the genes encoding the reduction-based iron uptake system. One could also speculate that because Fe^{3+} exists mostly as phytochelate in the apoplast (Sparla et al., 1999), this might have to be converted to Fe^{2+} by the reductase and could then be channeled efficiently to the high-affinity oxidase/permease system.

At present, we also cannot formally rule out the possibility that *fer2* could have additional roles besides providing iron for fungal growth in planta. It is conceivable that iron uptake is necessary to deplete iron from the environment to reduce the amount of iron available for the Fenton reaction, which could provide hydroxyl radicals from hydrogen peroxide, with potential harmful consequences to the fungus. However, diamino benzidine staining revealed no evidence for an accumulation of reactive oxygen species in tumor material from Δ*fer2* mutants (data not shown), despite the fact that such accumulations could readily be shown for mutant hyphae lacking a regulator for oxidative stress signaling (L. Molina and R. Kahmann, unpublished data).

So far, *U. maydis* is the only plant pathogenic fungus in which a ferroxidation/permeation iron uptake system is required for virulence. In this respect, *U. maydis* is similar to the human pathogen *C. albicans*, in which two high-affinity iron permeases, Ca *FTR1* and Ca *FTR2*, were identified and one of these, Ca *FTR2*, was shown to be essential for pathogenicity in a mouse model for systemic infection (Ramanan and Wang, 2000). Interestingly, the siderophore uptake system of *C. albicans* has subsequently been shown to play a role in epithelial invasion and penetration (Heymann et al., 2002). In the human pathogen *Aspergillus fumigatus*, the biosynthesis of siderophores is also essential for virulence, whereas the reductive iron assimilation system is not needed (Schrettl et al., 2004). To date, *Cochliobolus heterostrophus* is the only phytopathogenic fungus in which the production of siderophores has been shown to be required for virulence (Lee et al., 2005; Oide et al., 2006). However, this unique position is likely to change when the mode of iron acquisition in other plant pathogens is analyzed. One of the intriguing questions remaining is why phytopathogenic fungi use different strategies for iron acquisition during plant colonization. We consider it possible that the fungal lifestyle adopted after infection (i.e., to grow as a biotroph or necrotroph) may ultimately determine in which form the iron present in the host plant can be acquired. Another interesting avenue for future research will be to elucidate at which stages of its life cycle *U. maydis* makes use of the siderophore-mediated iron uptake system.

Table 2. Strains Used in This Study

Strain	Genotype	Reference
Ustilago maydis		
FB1	*a1b1*	Banuett and Herskowitz (1989)
FB2	*a2b2*	Banuett and Herskowitz (1989)
SG200	*a1mfa2bE1bW2*	Bölker et al. (1995)
FB1Δuac1	*a1b1Δuac1*	Krüger et al. (1998)
HE140	*a1b1*[P_{crg1}:*adr1*]*ip*^{s}	This work
FB1Δfer2	*a1b1Δfer2*	This work
FB2Δfer2	*a2b2Δfer2*	This work
FB1fer2:eGFP	*a1b1fer2:eGFP*	This work
FB2fer2:eGFP	*a2b2fer2:eGFP*	This work
FB1Δfer1	*a1b1Δfer1*	This work
FB2Δfer1	*a2b2Δfer1*	This work
BW12	*a1b1Δurbs1*	This work
Saccharomyces cerevisiae		
BY4741Δ*FTR1*	*MATaHIS3Δ1LEU2-Δ0MET15 Δ0URA3Δ0FTR1::KanMX*	Winzeler et al. (1999)

METHODS

Strains and Culture Conditions

The *Escherichia coli* K-12 derivative DH5α (Bethesda Research Laboratories) and Top10 (Invitrogen) were used as hosts for cloning purposes. The *Ustilago maydis* strains used and constructed are listed in Table 2. *U. maydis* strains were grown at 28°C in YEPSL medium (1% yeast extract, 0.4% trypton, and 0.4% sucrose) in low-iron medium (Sundström, 1964) or in CM (Holliday, 1974). $FeSO_4$ was added as indicated. For induction of the *crg1* promoter, cells were grown at 28°C in CM containing 1% glucose to an OD_{600} of 0.5, washed once with CM containing 1% arabinose, and then resuspended in prewarmed CM containing 1% arabinose. To assess spore viability, tumor material was dried, homogenized in a mortar, treated with a solution of 0.75% copper sulfate for 15 min, washed, spread on PD plates (3.9% potato dextrose agar and 0.01 M Tris-HCl, pH 8.0), and incubated for 2 d at 28°C. To test for mating, strains were cospotted on CM plates containing 1% activated charcoal and incubated at room temperature for 24 h. *Saccharomyces cerevisiae* strain BY4741ΔFTR1 was propagated in YPD medium containing yeast extract (10 g/L), peptone (10 g/L), and glucose (20 g/L), and transformants harboring plasmids pFtr1, pfer2, or Ycplac111-G/T were grown on plates lacking Leu (Guthrie and Fink, 1991). SD medium was prepared according to Ramanan and Wang (2000) with the following modifications: ferrozine was added to a final concentration of 2 mM, and $FeCl_3$ was added to final concentrations of 20 μM (SD20) or 50 μM (SD50) and contained either glucose (20 g/L) or galactose (20 g/L) as indicated.

Plant Infection Assays

Plant infections were done as described (Gillissen et al., 1992) with the maize (*Zea mays*) variety Early Golden Bantam. *U. maydis* strains were grown in YEPSL medium to an OD_{600} of 0.6 to 0.9, harvested, and resuspended in water to an OD_{600} of 2. For each mutant, between 30 and 40 plants (5-d-old seedlings) were syringe-infected with ~200 μL of the cell suspension. Plants were kept in a greenhouse (16 h of light, 28 to 32°C; 8 h of dark, 20°C), and symptoms were scored at different times after infection. Categories for disease rating were as follows: no symptoms, chlorosis, ligula swellings, small tumors of <1 mm in diameter, tumors of >1 mm in diameter that do not affect the growth axis of the plant, tumors of >1 mm in diameter that cause bending of infected stems, and dead plants. Based on the strongest symptoms, each infected plant was placed in one of these categories. Because of the high inoculum and the use of young maize seedlings for the infection, a high percentage of plants are killed by wild-type strains. Each plant infection experiment was done three times independently. Percentages given in Figure 5 represent averages of three experiments.

DNA and RNA Procedures

Standard molecular techniques followed Sambrook et al. (1989). *U. maydis* chromosomal DNA was isolated according to Hoffman and Winston (1987). Transformation of *U. maydis* followed the protocol of Schulz et al. (1990). Transformation of *S. cerevisiae* was done according to Guthrie and Fink (1991). RNA was isolated following the TRIZOL reagent protocol (Invitrogen). Probes for detecting transcripts from the iron gene clusters were generated by PCR and verified by diagnostic digestions. To generate probes for the *fer* genes, a 1-kb fragment was generated using the primer combination FL67 (5′-CGGACAGAACATCGGGTG-3′) and FL68 (5′-CCGTCCCCAAATCTGGTC-3′) for *fer1*; a 550-bp fragment was amplified with FL13 (5′-CTCACGACTCGCTTACCG-3′) and FL14 (5′-GAGGGTTCAGCTTCTCGG-3′) for *fer2*; a 650-bp fragment with primers FL61 (5′-CCCTTACCTCGCGTTCTG-3′) and FL62 (5′-GCGGAAGGCATCATCTGC-3′) for *fer4*; a 650-bp fragment with primers FL63 (5′-GAGACACCATGCAAGCCG-3′) and FL64 (5′-CCCTGTGAGACCGATCTC-3′) for *fer5*; a 1-kb fragment with primers FL31 (5′-CTCGCGGAACACTATGCG-3′) and FL32 (5′-CTGGGTGATGCCGAACAC-3′) for *fer6*; a 1.1-kb fragment with primers FL33 (5′-GCGTGATGCTGACGCTTC-3′) and FL34 (5′-GATCGTGCGTTACCTCCC-3′) for *fer7*; and an 800-bp fragment with primers FL65 (5′-GGGCGTCAAATGGGCTCAG-3′) and FL66 (5′-CGCTCGATCGATTCCCAG-3′) for *fer8*. To detect *sid1*, we generated an 800-bp fragment using primers FL5 (5′-GACCTCCTAGGTATCGGC-3′) and FL6 (5′-GCGCGGAAGATCATGGTG-3′). As a probe for *adr1*, a 1.2-kb *Nco*I-*Xho*I fragment was isolated from pMF35 (Kaffarnik et al., 2003). Probes for *pra1* and *mfa1* were as described (Müller et al., 2003). For radioactive labeling of DNA, the Megaprime DNA labeling kit (New England Biolabs) was used. Detection and quantification of the signals were done with the help of a STORM PhosphorImager and the ImageQuant program (Molecular Dynamics).

Plasmids and Plasmid Construction

pHEcrg:adr1

pHEcrg:adr1 was constructed by a three-fragment ligation: a 7.7-kb *Nde*I-*Eco*RI fragment from pRU11 (Brachmann et al., 2001) containing the carboxin resistance cassette and the *crg1* promoter fragment, a 1.1-kb *Nde*I-*Xho*I fragment from pMF35 containing the 5′ coding region of the *adr1* gene, and a 420-bp *Xho*I-*Eco*RI fragment from pMF35 containing the 3′ coding region of *adr1* including the 3′ untranslated region.

pΔfer2

To generate pΔfer2, two 1.0-kb fragments containing the 5′ region and the 3′ region of the *fer2* gene, respectively, were amplified by PCR using the primer combinations FL1 (5′-TTGTGGATGCAGGTGCGG-3′)/FL2 (5′-CACGGCCTGAGTGGCCCCGTTGCCGACATGTTTGC-3′) and FL3 (5′-GTGGGCCATCTAGGCCGGGTACTGGTTTGCCGTC-3′)/FL4 (5′-CGAAGCGTCAGGTACGTG-3′). The fragments were subsequently digested with *Sfi*I and ligated to the 2.7-kb *Sfi*I-digested hygromycin resistance cassette from plasmid pMF1-h (Brachmann et al., 2004) before cloning into pCR4-TOPO.

pfer2:eGFP

For the generation of pfer2:eGFP, two 1.0-kb fragments comprising the 3′ region and the 3′ untranslated region of *fer2* were amplified by PCR using the primer combinations FL52 (5′-CGCAGAGATGAAGAGGGC-3′)/FL53 (5′-ATAGGCCGCGTTGGCCGAGAGGGTACTTGGGCCAG-3′) and FL54 (5′-ATAGGCCTGAGTGGCCAGAGTGAATGCGCCAGCG-3′)/FL56 (5′-GGAGGTCACTCGACGAGTC-3′), respectively. The fragments were subsequently digested with *Sfi*I and ligated to the 3.7-kb *Sfi*I-digested eGFP–hygromycin resistance cassette from plasmid pMF5-h (Brachmann et al., 2004) before cloning into pCR4-TOPO.

fer1 Deletion Construct

To generate a fragment for the deletion of *fer1*, the 5′ and 3′ flanking regions of *fer1* were amplified with primer combinations HE148 (5′-CCGGCTCGCAAGTCAATC-3′)/HE149 (5′-CACGGCCTGAGTGGCCTTGCGAAGGTCGCCTAGG-3′) and HE150 (5′-GTGGGCCATCTAGGCCTGCATCATCACCGGCCTG-3′)/HE151 (5′-CTGAAGATCGTGGCGAGC-3′), respectively, before ligation to the 2.7-kb *Sfi*I hygromycin resistance cassette of plasmid pMF1-h. The deletion construct was amplified (Kämper, 2004) with primers HE148 and HE151.

pΔUrbs1

For the construction of pΔUrbs1, two 1.1-kb fragments comprising the 5′ and 3′ untranslated regions of *urbs1*, respectively, were generated by PCR using the oligonucleotide combinations oBW35 (5′-ATGTGCGTGTTGAGAAGACC-3′)/oBW36 (5′-TGACGGCCATCTAGGCCTTCTTGTCGTCCACGTATCC-3′) and oBW37 (5′-TAGCGGCCTGAGTGGCCAAGAAGGTGCCGCGATCTGC-3′)/oBW38 (5′-TTTGGCCCAGCTAAGAACC-3′) and digested with *Sfi*I before ligation to the 2.4-kb *Sfi*I fragment of pBS-hyg (Kämper, 2004) containing the hygromycin resistance cassette. The 4.6-kb ligation product was cloned into pCR2.1-TOPO (Invitrogen).

pFtr1

pFtr1 was generated by inserting a 1.2-kb *Bam*HI-*Sal*I fragment from plasmid pGAD-Ftr1 carrying the complete *FTR1* open reading frame into the respective sites of YCplac111-G/T. YCplac111-G/T is derived from plasmid YCplac111 (Gietz and Sugino, 1988) by insertion of the *GAL1* promoter and a transcriptional terminator (H.D. Ulrich, unpublished data). pGAD-Ftr1 is a derivative of the two-hybrid vector pGAD424 (Clontech) carrying the complete *FTR1* open reading frame (T. Albert and H.D. Ulrich, unpublished data).

pfer2

pfer2 was generated by inserting a 1.5-kb *Xba*I-*Pst*I fragment containing the coding region of *fer2* from plasmid pfer2ORF into YCplac111-G/T cleaved with the respective enzymes. pfer2ORF was generated by cloning the *fer2* cDNA generated from strain FB1 by RT-PCR using primers HE131 (5′-TTCTGCAGGGGCGAAAATGGGCTT-3′) and HE134 (5′-TATCTAGACCCGGGAATGTCGGCAACGGGCAAC-3′) into pCR4-TOPO. All fragments generated by PCR were sequenced to exclude mutations.

Generation of *U. maydis* Strains by Homologous Recombination

Strain HE140 was generated by integration of the pHEcrg1:adr1 linearized with *Ssp*I into the *ip* locus (Loubradou et al., 2001). FB1Δfer2 and FB2Δfer2 were generated from FB1 and FB2, respectively, by transformation with the *fer2* deletion construct generated by PCR from pΔfer2 using primers FL1 and FL4. The strains FB1fer2:eGFP and FB2fer2:eGFP were generated by transformation of the respective wild-type strains with a 5.7-kb *Eco*RI fragment from plasmid pfer2:eGFP. FB1Δfer1 and FB2Δfer1 were generated from FB1 and FB2, respectively, by transformation with the *fer1* deletion construct. Strain BW12 was generated from FB1 by transformation with the 4.6-kb PCR-amplified deletion construct derived from pΔurbs1 using the oligonucleotides oBW35 and oBW38. Single-copy integration of all constructs as well as homologous recombination was verified for all strains by diagnostic PCR and DNA gel blot analysis.

Sample Preparation and Microarray Analysis

Briefly, total RNA (for isolation, see above) was purified applying the RNeasy Mini kit (Qiagen). Purified RNA (10 μg) was reverse-transcribed using the Superscript Choice system (Invitrogen). The cDNA generated was purified using the GeneChip sample cleanup module (Qiagen) and transcribed in vitro with the ENZO BioArray High Yields RNA transcript 21 labeling kit (ENZO Diagnostics) using biotinylated ribonucleotides. Copy RNA was purified using the GeneChip sample cleanup module (Qiagen) and subsequently fragmented according to standard protocols (Affymetrix). The quality of RNA, cDNA, and copy RNA fragments was analyzed with an Agilent Bioanalyzer 2100 and RNA 6000 Nano LabChips or DNA 7500 LabChips, respectively (Agilent Technologies).

DNA array analysis was performed with custom-designed Affymetrix chips (MPIUstilagoA). Probe sets were designed based on a 17.4-Mb map-based sequencing assembly of the *U. maydis* genome of strain 521 (Bayer CropScience sequence; http://www.broad.mit.edu/annotation/genome/ustilago_maydis/). For each predicted gene, 33 perfect match and 33 corresponding mismatch probes were designed covering a region of 800 bp at the 3′ ends. The *U. maydis* DNA arrays address ~6300 of the 6902 predicted *U. maydis* genes. Genes not represented on the chip were recognized only after completion of the shotgun sequencing of *U. maydis* strain 521 by the Broad Institute (www.broad.mit.edu/annotation/fungi/ustilago_maydis/) and manual annotation by the Munich Information Center for Protein Sequences (MIPS). Probe sets for the individual genes have been integrated into the MIPS *Ustilago maydis* database and can be queried for individual genes at http://mips.gsf.de/genre/proj/ustilago/.

Hybridization was performed with fragmented copy RNA according to the Affymetrix protocol for eukaryotic targets on the Affymetrix custom array MPIUstilagoA. Subsequently, a three-stain procedure was performed according to the protocol EukGE-WS2 on a GeneChip Fluidics Station 400, which included signal amplification as well as washing steps (Affymetrix). Arrays were scanned twice using a GeneArray Scanner (Agilent/Affymetrix). The resulting image data were analyzed using the GeneChip Expression Analysis software (GCOS) Microarray Suite 5.0 (Affymetrix), using standard settings: Smooth factor, 100; Epsilon, 0.5; alpha1, 0.0575; alpha2, 0.0971; tau, 0.015; Gamma1H, 0.000423; Gamma1L, 0.000423; Gamma2H, 0.000627; Gamma2L, 0.000627; Perturbation, 1.1; TGT, 300. Further data analysis was performed using the Biconductor R package (http://www.bioconductor.org/). Expression values were converted to $\log_2$ (value + 1). Limma (Smyth, 2004) was used for the expression analysis of differentially regulated genes.

Using lmFit (Linear Model for Series of Arrays), a linear model was fitted to the $\log_2$ (value + 1) expression data for each probe, and contrasts.fit (Compute Contrasts from Linear Model Fit) was used to obtain coefficients and standard errors for contrasts of the coefficients of the original model. An empirical Bayes method, ebayes (Empirical Bayes Statistics for Differential Expression), was used to rank genes in order of evidence for differential expression. A table of the top-ranked genes from the linear model fit was extracted by topTable (Table of Top Genes from Linear Model Fit). The P values for the coefficients/contrasts of interest were adjusted for multiple testing by the Benjamini and Hochberg (1995) method fdr.

Genes with a corrected P value of <0.001 that were at least twofold regulated at either 75 or 180 min after induction were filtered by comparing HE140 and the FB1 control at the respective time points (biological triplicates each).

For the iron repression data set, genes were filtered with the following criteria: at least 1.5-fold regulated by the comparison of BW12 (FB1Δurbs1) with FB1 in the presence of 10 μM $FeSO_4$, and at least 1.5-fold regulated by the comparison of FB1 in the presence and absence of 10 μM $FeSO_4$ (biological duplicates each), and with a corrected P value of <0.05 in either of the two comparisons.

For cluster analysis, the dChip 1.2 software package (Li and Hung Wong, 2001a, 2001b; http://biosun1.harvard.edu/complab/dchip/) was used on gene lists generated by means of Bioconductor, and the expression values were calculated by MAS5.0 (dChip 1.2: hierarchical clustering) default settings: distance matrix, $1 - r$ (r is the Pearson correlation coefficient between standardized expression values), centroid linkage, gene ordering by cluster tightness (P value for significant cluster calls between genes, 0.001).

Sequence Analysis

Predicted amino acid sequences were analyzed using the programs BLASTP (Altschul et al., 1997), SMART (Schultz et al., 1998), and PFAM (Bateman et al., 2002).

Quantification of Iron

Iron quantification according to the method of Fish (1988) revealed that CM has an iron concentration of <0.8 μM, and the medium used to repress iron-responsive genes contained at least 10 μM $FeSO_4$.

Microscopy

Sections for microscopy were cut with a sharp razor blade from infected leaf tissue and were immersed in water immediately before microscopic observation. Calcofluor staining of fungal structures on the leaf surface and Chlorazole black E staining of infected plant leaf samples were performed as described (Brachmann et al., 2003). Samples were observed using a Zeiss Axiophot microscope with differential interference contrast optics or by epifluorescence microscopy with a specific filter set (BP470/20, FT 493, BP 505-530) for eGFP fluorescence. Pictures were taken using a CCD camera (C4742-95; Hamamatsu). Image processing and measurements were performed using Axiovision 3.1 (Zeiss) and Canvas 7.0 (Deneba).

Accession Numbers

Sequence data from this article can be accessed through the MIPS *Ustilago maydis* database (http://mips.gsf.de/genre/proj/ustilago/) and can be found in the GenBank/EMBL data libraries under accession numbers BK004082, BK004083, and BN000978. Microarray data files were submitted to the National Center for Biotechnology Information GEO database and can be accessed under accession numbers GSE6037, GSE6038, and GSE6039.

Supplemental Data

The following materials are available in the online version of this article.

Supplemental Figure 1. Hierarchical Cluster Analysis of Adr1-Regulated Genes.

Supplemental Table 1. List of Differentially Regulated Genes upon Arabinose-Induced Adr1 Expression in HE140.

Supplemental Table 2. List of Iron- and Urbs1-Repressed Genes as Deduced by Microarray Analysis.

ACKNOWLEDGMENTS

We thank Bayer CropScience for access to the *U. maydis* genome sequence before its public release. We thank N. von Wirén for maize *ys1* seeds. We acknowledge M. Vranes, M. Scherer, and J. Pons for expert advice on microarray technology and data analysis. We are grateful to H.D. Ulrich, T. Albert, and M. Feldbrügge for advice and for supplying plasmids and strains. We thank K. Münch and E. Meyer for expert technical assistance. This work was supported through a grant from the German Ministry for Science and Education.

Received April 25, 2006; revised October 18, 2006; accepted November 2, 2006; published November 30, 2006.

REFERENCES

Abramovitch, R.B., Yang, G., and Kronstad, J.W. (2002). The *ukb1* gene encodes a putative protein kinase required for bud site selection and pathogenicity in *Ustilago maydis.* Fungal Genet. Biol. **37,** 98–108.

Alspaugh, J.A., Perfect, J.R., and Heitman, J. (1997). *Cryptococcus neoformans* mating and virulence are regulated by the G-protein α subunit GPA1 and cAMP. Genes Dev. **11,** 3206–3217.

Altschul, S.F., Madden, T.L., Schaffer, A.A., Zhang, J., Zhang, Z., Miller, W., and Lipman, D.J. (1997). Gapped BLAST and PSI-BLAST: A new generation of protein database search programs. Nucleic Acids Res. **25,** 3389–3402.

An, Z., Mei, B., Yuan, W.M., and Leong, S.A. (1997). The distal GATA sequences of the *sid1* promoter of *Ustilago maydis* mediate iron repression of siderophore production and interact directly with Urbs1, a GATA family transcription factor. EMBO J. **16,** 1742–1750.

Ardon, O., Nudelman, R., Caris, C., Liebmann, J., Shanzer, A., Chen, Y., and Hadar, Y. (1998). Iron uptake in *Ustilago maydis*: Tracking the iron path. J. Bacteriol. **180,** 2021–2026.

Ardon, O., Weizman, H., Liebmann, J., Shanzer, A., Chen, Y., and Hadar, Y. (1997). Iron uptake in *Ustilago maydis*: Studies with fluorescent ferrichrome analogs. An. Microbiol. (Rio J.) **143,** 3625–3631.

Askwith, C., and Kaplan, J. (1997). An oxidase-permease-based iron transport system in *Schizosaccharomyces pombe* and its expression in *Saccharomyces cerevisiae.* J. Biol. Chem. **272,** 401–405.

Banuett, F., and Herskowitz, I. (1989). Different *a* alleles are necessary for maintenance of filamentous growth but not for meiosis. Proc. Natl. Acad. Sci. USA **86,** 5878–5882.

Banuett, F., and Herskowitz, I. (1996). Discrete developmental stages during teliospore formation in the corn smut fungus, *Ustilago maydis.* Development **122,** 2965–2976.

Barrett, K.J., Gold, S.E., and Kronstad, J.W. (1993). Identification and complementation of a mutation to constitutive filamentous growth in *Ustilago maydis.* Mol. Plant Microbe Interact. **6,** 274–283.

Bateman, A., Birney, E., Cerruti, L., Durbin, R., Etwiller, L., Eddy, S.R., Griffiths-Jones, S., Howe, K.L., Marshall, M., and Sonnhammer, E.L. (2002). The Pfam protein families database. Nucleic Acids Res. **30,** 276–280.

Benjamini, Y., and Hochberg, Y. (1995). Controlling the false discovery rate: A practical and powerful approach to multiple testing. J. R. Stat. Soc. Ser. B **57,** 289–300.

Bölker, M., Genin, S., Lehmler, C., and Kahmann, R. (1995). Genetic regulation of mating and dimorphism in *Ustilago maydis.* Can. J. Bot. **73,** 320–325.

Borges-Walmsley, M.I., and Walmsley, A.R. (2000). cAMP signalling in the pathogenic fungi: Control of dimorphic switching and pathogenicity. Trends Microbiol. **8,** 133–141.

Bottin, A., Kämper, J., and Kahmann, R. (1996). Isolation of a carbon source-regulated gene from *Ustilago maydis.* Mol. Gen. Genet. **253,** 342–352.

Brachmann, A., König, J., Julius, C., and Feldbrügge, M. (2004). A reverse genetic approach for generating gene replacement mutants in *Ustilago maydis.* Mol. Genet. Genomics **272,** 216–226.

Brachmann, A., Schirawski, J., Müller, P., and Kahmann, R. (2003). An unusual MAP kinase is required for efficient penetration of the plant surface by *Ustilago maydis.* EMBO J. **22,** 2199–2210.

Brachmann, A., Weinzierl, G., Kämper, J., and Kahmann, R. (2001). Identification of genes in the bW/bE regulatory cascade in *Ustilago maydis.* Mol. Microbiol. **42,** 1047–1063.

Budde, A.D., and Leong, S.A. (1989). Characterization of siderophores from *Ustilago maydis.* Mycopathologia **108,** 125–133.

Carniel, E. (2001). The *Yersinia* high-pathogenicity island: An iron-uptake island. Microbes Infect. **3,** 561–569.

Curie, C., Panavienne, Z., Loulergue, C., Dellaporta, S.L., Briat, J.-F., and Walker, E.L. (2001). Maize *yellow stripe1* encodes a membrane protein directly involved in Fe(III) uptake. Nature **409,** 346–349.

D'Souza, C.A., Alspaugh, J.A., Yue, C., Harashima, T., Cox, G.M., Perfect, J.R., and Heitman, J. (2001). Cyclic AMP-dependent protein

kinase controls virulence of the fungal pathogen *Cryptococcus neoformans.* Mol. Cell. Biol. **21,** 3179–3191.

Dürrenberger, F., Laidlaw, R.D., and Kronstad, J.W. (2001). The *hgl1* gene is required for dimorphism and teliospore formation in the fungal pathogen *Ustilago maydis.* Mol. Microbiol. **41,** 337–348.

Dürrenberger, F., Wong, K., and Kronstad, J.W. (1998). Identification of a cAMP-dependent protein kinase catalytic subunit required for virulence and morphogenesis in *Ustilago maydis.* Proc. Natl. Acad. Sci. USA **95,** 5684–5689.

Ecker, D., and Emery, T. (1983). Iron uptake from ferrichrome A and iron citrate in *Ustilago sphaerogena.* J. Bacteriol. **155,** 616–622.

Eisendle, M., Oberegger, H., Zadra, I., and Haas, H. (2003). The siderophore system is essential for viability of *Aspergillus nidulans*: Functional analysis of two genes encoding L-ornithine N^5-monooxygenase (*sidA*) and a non-ribosomal peptide synthetase (*sidC*). Mol. Microbiol. **49,** 359–375.

Fang, H.-M., and Wang, Y. (2002). Characterization of iron-binding motifs in *Candida albicans* high-affinity iron permease CaFtr1p by site-directed mutagenesis. Biochem. J. **368,** 641–647.

Fish, W.W. (1988). Rapid colorimetric micromethod for the quantitation of complexed iron in biological samples. Methods Enzymol. **158,** 357–364.

Georgatsou, E., and Alexandraki, D. (1994). Two distinctly regulated genes are required for ferric reduction, the first step of iron uptake in *Saccharomyces cerevisiae.* Mol. Cell. Biol. **14,** 3065–3073.

Gietz, R.D., and Sugino, A. (1988). New yeast-*Escherichia coli* shuttle vectors constructed with in vitro mutagenized yeast genes lacking six-base pair restriction sites. Gene **74,** 527–534.

Gillissen, B., Bergemann, J., Sandmann, C., Schröer, B., Bölker, M., and Kahmann, R. (1992). A two-component regulatory system for self/non-self recognition in *Ustilago maydis.* Cell **68,** 647–657.

Gold, S., Duncan, G., Barrett, K., and Kronstad, J. (1994). cAMP regulates morphogenesis in the fungal pathogen *Ustilago maydis.* Genes Dev. **8,** 2805–2816.

Gold, S.E., Brogdon, S.M., Mayorga, M.E., and Kronstad, J.W. (1997). The *Ustilago maydis* regulatory subunit of a cAMP-dependent protein kinase is required for gall formation in maize. Plant Cell **9,** 1585–1594.

Guthrie, C., and Fink, G.R. (1991). Guide to Yeast Genetics and Molecular Biology. Methods Enzymol. **194,** 13–37.

Haas, H. (2003). Molecular genetics of fungal siderophore biosynthesis and uptake: The role of siderophores in iron uptake and storage. Appl. Microbiol. Biotechnol. **62,** 316–330.

Hartmann, H.A., Krüger, J., Lottspeich, F., and Kahmann, R. (1999). Environmental signals controlling sexual development of the corn smut fungus *Ustilago maydis* through the transcriptional regulator Prf1. Plant Cell **11,** 1239–1305.

Heymann, P., Gerads, M., Schaller, M., Dromer, F., Winkelmann, G., and Ernst, J.F. (2002). The siderophore iron transporter of *Candida albicans* (Sit1p/Arn1p) mediates uptake of ferrichrome-type siderophores and is required for epithelial invasion. Infect. Immun. **70,** 5246–5255.

Hoffman, C.S., and Winston, F. (1987). A ten-minute DNA preparation from yeast efficiently releases autonomous plasmids for transformation of *E. coli.* Gene **57,** 267–272.

Holliday, R. (1974). *Ustilago maydis.* In Handbook of Genetics, Vol. 1, R.C. King, ed (New York: Plenum Press), pp. 575–595.

Irie, T., Matsumura, H., Terauchi, R., and Saitoh, H. (2003). Serial analysis of gene expression (SAGE) of *Magnaporthe grisea*: Genes involved in appressorium formation. Mol. Genet. Genomics **270,** 181–189.

Kaffarnik, F., Müller, P., Leibundgut, M., Kahmann, R., and Feldbrügge, M. (2003). PKA and MAPK phosphorylation of Prf1 allows promoter discrimination in *Ustilago maydis.* EMBO J. **22,** 5817–5826.

Kahmann, R., Steinberg, G., Basse, C., Feldbrügge, M., and Kämper, J. (2000). *Ustilago maydis*, the causative agent of corn smut disease. In Fungal Pathology, J.W. Kronstad, ed (Dordrecht, the Netherlands: Kluwer Academic Publishers), pp. 347–371.

Kämper, J. (2004). A PCR-based system for highly efficient generation of gene replacement mutants in *Ustilago maydis.* Mol. Genet. Genomics **271,** 103–110.

Kosman, D.J. (2003). Molecular mechanisms of iron uptake in fungi. Mol. Microbiol. **47,** 1185–1197.

Krüger, J., Loubradou, G., Regenfelder, E., Hartmann, A., and Kahmann, R. (1998). Crosstalk between cAMP and pheromone signalling pathways in *Ustilago maydis.* Mol. Gen. Genet. **260,** 193–198.

Krüger, J., Loubradou, G., Wanner, G., Regenfelder, E., Feldbrugge, M., and Kahmann, R. (2000). Activation of the cAMP pathway in *Ustilago maydis* reduces fungal proliferation and teliospore formation in plant tumors. Mol. Plant Microbe Interact. **13,** 1034–1040.

Labudova, O., and Lubec, G. (1998). cAMP up-regulates the transposable element mys-1: A possible link between signaling and mobile DNA. Life Sci. **62,** 431–437.

Lan, C.Y., Rodarte, G., Murillo, L.A., Jones, T., Davis, R.W., Dungan, J., Newport, G., and Agabian, N. (2004). Regulatory networks affected by iron availability in *Candida albicans.* Mol. Microbiol. **53,** 1451–1469.

Larraya, L.M., Boyce, K.J., So, A., Steen, B.R., Jones, S., Marra, M., and Kronstad, J.W. (2005). Serial analysis of gene expression reveals conserved links between protein kinase A, ribosome biogenesis, and phosphate metabolism in *Ustilago maydis.* Eukaryot. Cell **4,** 2029–2043.

Lee, B.N., Kroken, S., Chou, D.Y., Robbertse, B., Yoder, O.C., and Turgeon, B.G. (2005). Functional analysis of all nonribosomal peptide synthetases in *Cochliobolus heterostrophus* reveals a factor, NPS6, involved in virulence and resistance to oxidative stress. Eukaryot. Cell **4,** 545–555.

Lee, N., D'Souza, C.A. and Kronstad, J.W. (2003). Of smuts, blasts, mildews, and blights: cAMP signalling in phytopathogenic fungi. Annu. Rev. Phytopathol. **41,** 03.1–03.29.

Li, C., and Hung Wong, W. (2001a). Model-based analysis of oligonucleotide arrays: Expression index computation and outlier detection. Proc. Natl. Acad. Sci. USA **98,** 31–36.

Li, C., and Hung Wong, W. (2001b). Model-based analysis of oligonucleotide arrays: Model validation, design issues and standard error application. Genome Biol. **2,** RESEARCH0032.

Lian, T., Simmer, M.I., D'Souza, C.A., Steen, B.R., Zuyderduyn, S.D., Jones, S.J.M., Marra, M.A., and Kronstad, J.W. (2005). Iron-regulated transcription and capsule formation in the fungal pathogen *Cryptococcus neoformans.* Mol. Microbiol. **55,** 1452–1472.

Loubradou, G., Brachmann, A., Feldbrügge, M., and Kahmann, R. (2001). A homologue of the transcriptional repressor Ssn6p antagonizes cAMP signalling in *Ustilago maydis.* Mol. Microbiol. **40,** 719–730.

Mayorga, M.E., and Gold, S. (2001). The *ubc2* gene of *Ustilago maydis* encodes a putative novel adaptor protein required for filamentous growth, pheromone response and virulence. Mol. Microbiol. **41,** 1365–1379.

Mei, B., Budde, A.D., and Leong, S.A. (1993). *sid1*, a gene initiating siderophore biosynthesis in *Ustilago maydis*: Molecular characterization, regulation by iron, and role in phytopathogenicity. Proc. Natl. Acad. Sci. USA **90,** 903–907.

Müller, P., Aichinger, C., Feldbrügge, M., and Kahmann, R. (1999). The MAP kinase *kpp2* regulates mating and pathogenic development in *Ustilago maydis.* Mol. Microbiol. **34,** 1007–1017.

Müller, P., Weinzierl, G., Brachmann, A., Feldbrügge, M., and Kahmann, R. (2003). Both mating and pathogenic development of

the smut fungus *Ustilago maydis* are regulated by one MAP kinase cascade. Eukaryot. Cell **2,** 1187–1199.

Oide, S., Moeder, W., Krasnoff, S., Gibson, D., Haas, H., Yoshioka, K., and Turgeon, B.G. (2006). NPS6, encoding a nonribosomal peptide synthetase involved in siderophore-mediated iron metabolism, is a conserved virulence determinant of plant pathogenic Ascomycetes. Plant Cell **18,** 2836–2853.

Ramanan, N., and Wang, Y. (2000). A high-affinity iron permease essential for *Candida albicans* virulence. Science **288,** 1062–1064.

Regenfelder, E., Spellig, T., Hartmann, A., Lauenstein, S., Bölker, M., and Kahmann, R. (1997). G proteins in *Ustilago maydis*: Transmission of multiple signals? EMBO J. **16,** 1934–1942.

Robertson, L.S., Causton, H.C., Young, R.A., and Fink, G.R. (2000). The yeast A kinases differentially regulate iron uptake and respiratory function. Proc. Natl. Acad. Sci. USA **97,** 5984–5988.

Rodriguez, G.M., and Smith, I. (2003). Mechanisms of iron regulation in mycobacteria: Role in physiology and virulence. Mol. Microbiol. **47,** 1485–1494.

Rutherford, J.C., and Bird, A.J. (2004). Metal-responsive transcription factors that regulate iron, zinc, and copper homeostasis in eukaryotic cells. Eukaryot. Cell **3,** 1–13.

Sambrook, J., Frisch, E.F., and Maniatis, T. (1989). Molecular Cloning: A Laboratory Manual. (Cold Spring Harbor, NY: Cold Spring Harbor Laboratory Press).

Schrettl, M., Bignell, E., Kragl, C., Joechl, C., Rogers, T., Arst, H.N., Jr., Haynes, K., and Haas, H. (2004). Siderophore biosynthesis but not reductive iron assimilation is essential for *Aspergillus fumigatus* virulence. J. Exp. Med. **200,** 1213–1219.

Schryvers, A.B., and Stojiljkovic, I. (1999). Iron acquisition systems in the pathogenic Neisseria. Mol. Microbiol. **32,** 1117–1123.

Schultz, J., Milpetz, F., Bork, P., and Ponting, C.P. (1998). SMART, a simple modular architecture research tool: Identification of signaling domains. Proc. Natl. Acad. Sci. USA **95,** 5857–5864.

Schulz, B., Banuett, F., Dahl, M., Schlesinger, R., Schäfer, W., Martin, T., Herskowitz, I., and Kahmann, R. (1990). The *b* alleles of *U. maydis*, whose combinations program pathogenic development, code for polypeptides containing a homeodomain-related motif. Cell **60,** 295–306.

Schwecke, T., Göttling, K., Durek, P., Dueñas, I., Käufer, N.F., Zock-Emmenthal, S., Staub, E., Neuhof, T., Dieckmann, R., and von Döhren, H. (2006). Nonribosomal peptide synthesis in *Schizosaccharomyces pombe* and the architectures of ferrichrome-type siderophore synthetases in fungi. ChemBioChem **7,** 612–622.

Smyth, G.K. (2004). Linear models and empirical Bayes methods for assessing differential expression in microarray experiments. Stat. Appl. Genet. Mol. Biol. **3,** Article 3.

Snetselaar, K.M., and Mims, C.W. (1994). Light and electron microscopy of *Ustilago maydis* hyphae in maize. Mycol. Res. **98,** 347–355.

Sparla, F., Preger, V., Pupillo, P., and Trost, P. (1999). Characterization of a novel NADH-specific, FAD-containing, soluble reductase with ferric citrate reductase activity from maize seedlings. Arch. Biochem. Biophys. **363,** 301–308.

Sundström, K.-R. (1964). Studies of the physiology, morphology and serology of exobasidium. Symb. Bot. Ups. **XVIII,** 3.

Voisard, C., Wang, J., McEvoy, J.L., Xu, P., and Leong, S.A. (1993). *urbs1*, a gene regulating siderophore biosynthesis in *Ustilago maydis*, encodes a protein similar to the erythroid transcription factor GATA-1. Mol. Cell. Biol. **13,** 7091–7100.

Wang, J., Budde, A.D., and Leong, S.A. (1989). Analysis of ferrichrome biosynthesis in the phytopathogenic fungus *Ustilago maydis*: Cloning of an ornithine-N^5-oxygenase gene. J. Bacteriol. **171,** 2811–2818.

Welzel, K., Eisfeld, K., Antelo, L., Anke, T., and Anke, H. (2005). Characterization of the ferrichrome A biosynthetic gene cluster in the homobasidiomycete *Omphalotus olearius.* FEMS Microbiol. Lett. **249,** 157–163.

Winkelmann, G. (2002). Microbial siderophore-mediated transport. Biochem. Soc. Trans. **30,** 691–696.

Winzeler, E.A., et al. (1999). Functional characterization of the *Saccharomyces cerevisiae* genome by gene deletion and parallel analysis. Science **285,** 901–906.

Yamaguchi-Iwai, Y., Stearman, R., Dancis, A., and Klausner, R.D. (1996). Iron-regulated DNA binding by the AFT1 protein controls the iron regulon in yeast. EMBO J. **15,** 3377–3384.

Yuan, W.M., Gentil, G.D., Budde, A.D., and Leong, S.A. (2001). Characterization of the *Ustilago maydis sid2* gene, encoding a multidomain peptide synthetase in the ferrichrome biosynthetic gene cluster. J. Bacteriol. **183,** 4040–4051.

Znaidi, S., Pelletier, B., Mukai, Y., and Labbe, S. (2004). The *Schizosaccharomyces pombe* corepressor Tup11 interacts with the iron-responsive transcription factor Fep1. J. Biol. Chem. **279,** 9462–9474.